*Mathematical Methods in the Applied Sciences*

WILEY

RESEARCH ARTICLE OPEN ACCESS

# An Inverse Source Technique as a Preliminary Tool to Localize Persons in Indoor Spaces

Simonetta Boria | Nadaniela Egidi | Lorella Fatone | Josephin Giacomini | Pierluigi Maponi | Riccardo Piombin

School of Science and Technology, University of Camerino (UNICAM), Camerino, Italy

**Correspondence:** Riccardo Piombin (riccardo.piombin@unicam.it)

**Received:** 18 December 2024 | **Revised:** 28 July 2025 | **Accepted:** 26 August 2025

**Funding:** This research received partial funding from Unione Europea-FSE, through Ministero dell'Università e della Ricerca within the call for the project Pon Ricerca e Innovazione 2014-2020 in Decreto Ministeriale 1062-10/08/2021. This research has received funding from the PNRR Ecosystem Project - Vitality Spoke 5 - CUP J13C22000430001.

**Keywords:** Green's function | inverse source problem | person localization

## ABSTRACT

This paper considers an inverse heat source localization problem with applications to indoor person localization from temperature measurements. In particular, this inverse problem consists in the reconstruction of the intensity and position of heat sources from observed temperature data. The proposed approach leverages the Green function method to model the heat distribution in three-dimensional intervals. This approach allows the formulation of the considered inverse problem through a Volterra integral equation, so numerical quadrature and Tikhonov regularization are employed in the approximation procedure. The validation of the proposed method is conducted through numerical experiments with synthetic data, where various configurations of heat sources in controlled indoor environments have been tested. Results demonstrate the method robustness and accuracy in localizing active heat sources while maintaining privacy and requiring minimal computational resources. Potential applications extend to smart living environments and noninvasive occupant detection also including safety issues.

## 1 | Introduction

The inverse heat source problem deals with the determination of the position and intensity of unknown heat sources within a given domain from some knowledge of the temperature distribution. The applications of the inverse heat source problem are vast and diverse. Interesting examples are the detection of abnormal heat sources in thermography analyses [1] and pollution detection [2]. Generally, in engineering, inverse problems have found a significant development [3]. Additionally, heat source localization can be important to provide a better understanding of different medium's behavior [4, 5]. The localization of heat sources has been also studied by using acoustic pressure measurements [6] and by analyzing temperature measurements on heat conducting objects [7, 8].

This problem does not have a straightforward formulation since it is stated in terms of the direct problem, that is, the initial-boundary value problem for heat equation describing the effect of the sources on the temperature distribution. As opposed to other inverse problems, that generally are not ill-posed [9], however, regularization techniques can be used to stabilize and improve the numerical results obtained by the inverse procedure. To this aim, one of the most used stabilization approaches is the Tikhonov regularization technique [10]. Furthermore, extensions and modifications of Tikhonov regularization technique, such as iterative and adaptive schemes, have enhanced its applicability to various problems [11, 12]. This stabilization procedure applies straightforwardly within the optimization methods, such as least squares [13, 14], which are utilized to identify the heat sources by minimizing the discrepancy between

observed and computed temperature fields in the so-called direct approach.

An important method to solve such inverse problems involves the use of the Green function of the differential operators that describe the boundary value problem under study. The Green functions give the integral representation of the solution of these boundary value problems. So they are a powerful tool for solving the inverse heat source problem by transforming this problem into an integral equation, usually a Volterra integral equation of the first kind [15, 16], allowing in this way the exploitation of the wide literature on the numerical solution of the Volterra integral equations [17, 18]. Moreover, for such equations, an interesting survey of regularization methods has been proposed [19].

Our study arose from an application in the living sector, with the final aim of localizing indoor space occupants through the acquisition of room temperature data via sensors positioned on the ceiling [20]. In the proposed method, the heat source of the human body has been approximated by a gaussian shaped heat source. In fact, the smoothing properties of the heat operator tend to cancel the details in the initial data and in the source data (far from its support). So, this is a perfect localization tool in sensible situations like elementary schools or kindergartens, where privacy issues require special attention. So, the main advantages of this method are the requirement of very simple measurement tools and the ability of being employed without privacy concerns. While the work done in [20] uses a least-square approach with real data to localize the heat sources, for this case study, we propose the Green function approach to construct a Volterra equation of the first kind with the aim of determining the intensity of sources. This integral equation is discretized through the trapezoidal quadrature rule, leading to a linear system whose numerical solution is stabilized by the Tikhonov regularization technique. The proposed method has been tested with numerical experiments where synthetic data are used.

The paper is structured as follows: Section 2 describes the mathematical model for the considered problem and the formulation of its solution, beginning with the one-dimensional case to introduce the main concepts and then extending these arguments to three dimensions. The Green function approach and its integral representation are discussed in detail, alongside numerical techniques for integral approximation. Section 3 formulates the inverse problem, focusing on the reconstruction of heat source intensities from temperature measurements. This section also outlines the regularization strategies employed for the problem. Section 4 presents numerical experiments with different heat source configurations, demonstrating the accuracy and robustness of the proposed method. Finally, Section 5 provides some conclusions and a discussion on future developments of this work.

## 2 | Model Formulation

Let $\mathbb{R}$ and $\mathbb{C}$ be the set of real numbers and complex numbers, respectively. Let $n$ be a positive integer, $\mathbb{R}^n$ represents the $n$-dimensional real Euclidean space, and vectors in $\mathbb{R}^n$ are indicated in bold throughout this paper.

We define the initial-boundary problem for the heat equation from which the inverse source problem under consideration is obtained. We describe the Green function method [21] for the solution of this initial-boundary problem and the integral formulation of its solution. The one-dimensional case is used to introduce the main ideas and mathematical details that are then generalized to the three-dimensional case. In Section 2.1, the one-dimensional problem is formulated. The Green function approach is applied to express the solution with an integral representation. In Section 2.2, computational details for the integral approximation are outlined, emphasizing the importance of the source function choice to handle singularities effectively. Finally, in Section 2.3, the three-dimensional problem is formulated.

### 2.1 | One-Dimensional Problem

Let $\Omega = [0, L] \subset \mathbb{R}$, $L > 0$ be the one dimensional spatial domain, $[0, T]$ be the time interval, and $u(x, t)$ be the function representing the temperature value at a point $x \in \Omega$ and time $t \in [0, T]$. We consider the following problem:

$$\begin{cases} \frac{\partial u}{\partial t}(x,t) - \alpha \frac{\partial^2 u}{\partial x^2}(x,t) = f(x,t), & x \in \Omega,\ t \in (0,T), \\ \frac{\partial u}{\partial x}(0,t) = 0, & t \in [0,T], \\ \frac{\partial u}{\partial x}(L,t) = 0, & t \in [0,T], \\ u(x,0) = u_0(x), & x \in \Omega, \end{cases} \tag{1}$$

where $\alpha \in \mathbb{R}$, $\alpha > 0$, is a constant representing the thermal diffusivity, $u_0(x)$ is the initial temperature, that is, the temperature at time $t = 0$, and $f(x, t)$ is the function representing the source term. From standard arguments on the differential equation theory, we have that the solution of problem (1) can be expressed in the following form [22]:

$$u(x,t) = \int_0^L G(x,t;\xi,0)u_0(\xi)d\xi + \int_0^t \left( \int_0^L G(x,t;\xi,\tau)f(\xi,\tau)d\xi \right) d\tau. \tag{2}$$

For $x, \xi \in \Omega$ and $t, \tau \in [0, T]$, the function $G(x, t; \xi, \tau)$ is the Green function associated to problem (1); in particular, it is the solution of the following auxiliary problem:

$$\begin{cases} \frac{\partial G}{\partial t}(x,t;\xi,\tau) - \alpha \frac{\partial^2 G}{\partial x^2}(x,t;\xi,\tau) \\ \qquad = \delta(x-\xi)\delta(t-\tau), & x \in \Omega,\ t \in (0,T), \\ \frac{\partial G}{\partial x}(0,t;\xi,\tau) = 0, & t \in [0,T], \\ \frac{\partial G}{\partial x}(L,t;\xi,\tau) = 0, & t \in [0,T], \\ G(x,0;\xi,\tau) = 0, & x \in \Omega, \end{cases} \tag{3}$$

where $\delta(\cdot)$ denotes the Dirac delta distribution.

We can express the solution of problem (3) in the following form:

$$G(x,t;\xi,\tau) = K(x,t;\xi,\tau) + v(x,t;\xi,\tau) \tag{4}$$

where $K(x,t;\xi,\tau)$ is the heat kernel [23] , given by the following:

$$K(x,t;\xi,\tau)=\begin{cases}\frac{1}{\sqrt{4\pi\alpha(t-\tau)}}e^{-\frac{(x-\xi)^2}{4\alpha(t-\tau)}} & t-\tau>0,\\ 0 & t-\tau\le 0,\end{cases} \tag{5}$$

and $v(x,t;\xi,\tau)$ is an unknown function that must be determined to prescribe the boundary conditions in (3). By replacing $G(x,t;\xi,\tau)$, given in (4), into problem (3), we obtain that $v(x,t;\xi,\tau)$ must satisfy the following boundary value problem

$$\begin{cases}\frac{\partial v}{\partial t}(x,t;\xi,\tau)-\alpha\frac{\partial^2 v}{\partial x^2}(x,t;\xi,\tau)=0, & x\in\Omega,\ t\in(0,T),\\ \frac{\partial v}{\partial x}(0,t;\xi,\tau)=-\frac{\partial K}{\partial x}(0,t;\xi,\tau), & t\in[0,T],\\ \frac{\partial v}{\partial x}(L,t;\xi,\tau)=-\frac{\partial K}{\partial x}(L,t;\xi,\tau), & t\in[0,T],\\ v(x,0;\xi,\tau)=0, & x\in\Omega.\end{cases} \tag{6}$$

We note that $K$ only depends from the time variable through the difference $t-\tau\ge 0$. So, the solution $v$ of problem (6) is supposed to have the same dependence from $t$; in particular, we assume that

$$v(x,t;\xi,\tau)=V(x,t-\tau;\xi),$$

for a suitable function $V$. So, we can consider the Laplace transform with respect to $t-\tau$ of the functions $v(x,t;\xi,\tau)$ and $K(x,t;\xi,\tau)$, that is, $\overline{v}(x,\xi,s)$ and $\overline{K}(x,\xi,s)$; so, for example, we have that

$$\overline{v}(x,\xi,s)=\int_0^{+\infty}e^{-st'}V(x,t';\xi)dt'.$$

From the properties of the Laplace transform and from (4), we have the following:

$$\overline{G}(x,\xi,s)=\overline{K}(x,\xi,s)+\overline{v}(x,\xi,s) \tag{7}$$

where [24]

$$\overline{K}(x,\xi,s)=\frac{1}{2\sqrt{\alpha s}}e^{-\sqrt{\frac{s}{\alpha}}|x-\xi|} \tag{8}$$

From problem (6) and the properties of the Laplace transform, we have the following:

$$\begin{cases}\frac{\partial^2\overline{v}}{\partial x^2}(x,\xi,s)-\frac{s}{\alpha}\overline{v}(x,\xi,s)=0,\\ \frac{\partial\overline{v}}{\partial x}(0,\xi,s)=-\frac{\partial\overline{K}}{\partial x}(0,\xi,s),\\ \frac{\partial\overline{v}}{\partial x}(L,\xi,s)=-\frac{\partial\overline{K}}{\partial x}(L,\xi,s),\end{cases} \tag{9}$$

where $s\in\mathbb{C}$ and we have supposed the commutative property between the derivatives with respect to $x$ and the Laplace operator. Hence, we have

$$\overline{v}(x,\xi,s)=a_+e^{\sqrt{\frac{s}{\alpha}}x}+a_-e^{-\sqrt{\frac{s}{\alpha}}x} \tag{10}$$

Moreover, constants $a_+$ and $a_-$ can be found by imposing the boundary conditions. In particular, we have the following:

$$\sqrt{\frac{s}{\alpha}}a_+-\sqrt{\frac{s}{\alpha}}a_-=-\frac{1}{2\alpha}e^{-\sqrt{\frac{s}{\alpha}}\xi},$$

and

$$\sqrt{\frac{s}{\alpha}}a_+e^{\sqrt{\frac{s}{\alpha}}L}-\sqrt{\frac{s}{\alpha}}a_-e^{-\sqrt{\frac{s}{\alpha}}L}=\frac{1}{2\alpha}e^{-\sqrt{\frac{s}{\alpha}}(L-\xi)},$$

whose solution is

$$a_+=\frac{1}{2\sqrt{\alpha s}}\left(\frac{e^{-\sqrt{\frac{s}{\alpha}}(L-\xi)}+e^{-\sqrt{\frac{s}{\alpha}}(\xi+L)}}{e^{\sqrt{\frac{s}{\alpha}}L}-e^{-\sqrt{\frac{s}{\alpha}}L}}\right),$$

$$a_-=\frac{1}{2\sqrt{\alpha s}}\left(\frac{e^{-\sqrt{\frac{s}{\alpha}}(L-\xi)}+e^{-\sqrt{\frac{s}{\alpha}}(\xi-L)}}{e^{\sqrt{\frac{s}{\alpha}}L}-e^{-\sqrt{\frac{s}{\alpha}}L}}\right).$$

By substituting $a_+$ and $a_-$ into $\overline{v}$, we obtain the following:

$$\overline{v}(x,\xi,s)=\frac{1}{\sqrt{4\alpha s}}\left(\frac{e^{-\sqrt{\frac{s}{\alpha}}(L-\xi-x)}+e^{-\sqrt{\frac{s}{\alpha}}(L-\xi+x)}+e^{-\sqrt{\frac{s}{\alpha}}(L+\xi-x)}+e^{-\sqrt{\frac{s}{\alpha}}(-L+\xi+x)}}{e^{\sqrt{\frac{s}{\alpha}}L}-e^{-\sqrt{\frac{s}{\alpha}}L}}\right), \tag{11}$$

and finally, by using (11) and (8) in (7), we obtain the following:

$$\overline{G}(x,\xi,s)=\frac{1}{\sqrt{4\alpha s}}e^{-\sqrt{\frac{s}{\alpha}}|x-\xi|}+\frac{1}{\sqrt{4\alpha s}}\cdot\left(\frac{e^{-\sqrt{\frac{s}{\alpha}}(L-\xi-x)}+e^{-\sqrt{\frac{s}{\alpha}}(L-\xi+x)}+e^{-\sqrt{\frac{s}{\alpha}}(L+\xi-x)}+e^{-\sqrt{\frac{s}{\alpha}}(-L+\xi+x)}}{e^{\sqrt{\frac{s}{\alpha}}L}-e^{-\sqrt{\frac{s}{\alpha}}L}}\right). \tag{12}$$

The inverse Laplace transform of function $\overline{G}$ in (12) gives the required function G; in (12), the inverse transform of the first term gives the fundamental solution $K$ (see (8)), whereas the second addendum has not an explicit inverse transform; however, we can implement an approach similar to the one used in [25]. In particular, for the denominator in this term, we can use the geometric series

$$\frac{1}{e^{\sqrt{\frac{s}{\alpha}}L}-e^{-\sqrt{\frac{s}{\alpha}}L}}=\frac{1}{e^{\sqrt{\frac{s}{\alpha}}L}}\cdot\frac{1}{1-e^{-2L\sqrt{\frac{s}{\alpha}}}}=\frac{1}{e^{\sqrt{\frac{s}{\alpha}}L}}\sum_{n=0}^{+\infty}\left(e^{-2L\sqrt{\frac{s}{\alpha}}}\right)^n;$$

thus,

$$\overline{v}(x,\xi,s)=\frac{1}{\sqrt{4\alpha s}}\sum_{n=0}^{+\infty}\left(e^{-\sqrt{\frac{s}{\alpha}}(2L+2Ln+\xi-x)}+e^{-\sqrt{\frac{s}{\alpha}}(2L+2Ln-\xi-x)}+e^{-\sqrt{\frac{s}{\alpha}}(2Ln+\xi+x)}+e^{-\sqrt{\frac{s}{\alpha}}(2L+2Ln-\xi+x)}\right).$$

In this way, we can consider the explicit inverse transform of $\overline{v}$, through the table of Laplace transforms [24], and obtain

$$v(x,t;\xi,\tau)=\frac{1}{\sqrt{4\alpha\pi(t-\tau)}}\sum_{n=0}^{+\infty}\left(e^{-\frac{(2L+2Ln+\xi-x)^2}{4\alpha(t-\tau)}}+e^{-\frac{(2L+2Ln-\xi-x)^2}{4\alpha(t-\tau)}}+e^{-\frac{(2Ln+\xi+x)^2}{4\alpha(t-\tau)}}+e^{-\frac{(2L+2Ln-\xi+x)^2}{4\alpha(t-\tau)}}\right). \tag{13}$$

Finally, by using (4), the Green function can be approximated as follows:

$$G(x,t;\xi,\tau)\approx\frac{1}{\sqrt{4\pi\alpha(t-\tau)}}\left[g(y_1,\mathcal{T})+\sum_{n=0}^{N}\sum_{h=2}^{5}g(y_{h,n},\mathcal{T})\right], \tag{14}$$

where $\mathcal{T} = 4\alpha(t-\tau)$, $N$ is a given truncation parameter of the series in (13), and

$$g(y,\mathcal{T}) = e^{-\frac{y^2}{\mathcal{T}}}, \qquad y_1 = x - \xi, \tag{15}$$

and for $n = 0, \dots, N$,

$$\begin{aligned} y_{2,n} &= 2L + 2Ln + \xi - x, \\ y_{3,n} &= 2L + 2Ln - \xi - x, \\ y_{4,n} &= 2Ln + \xi + x, \\ y_{5,n} &= 2L + 2Ln - \xi + x. \end{aligned}$$

We note that, from the knowledge of $G$, the solution $u(x,t)$ of problem (1) is given by (2).

### 2.2 | A Note on the Computational Details of Formula (2)

The integral representation (2) has a key role in the inverse problem. So, its numerical approximation has to be done in an efficient way. The first integral

$$\int_0^L G(x,t;\xi,0)u_0(\xi)d\xi$$

is approximated through the trapezoidal rule [26]. This method has been chosen for its effectiveness in approximating definite integrals, especially when the computational cost is a critical element as in the real-time application mentioned in the introduction.

The second integral

$$\int_0^t \left( \int_0^L G(x,t;\xi,\tau) f(\xi,\tau) d\xi \right) d\tau$$

requires special attention because of its singularity at $\tau = t$. In the following, we consider a particular form for the function $f(x,t)$

$$f(x,t) = \frac{1}{\sqrt{2\pi}} \sum_{m=1}^{M} \sigma_m(t) f_m(x) \tag{16}$$

where

$$f_m(x) = e^{-\epsilon_m^2 (x - x_m)^2} \tag{17}$$

In other words, the source $f(x,t)$ is supposed to be equal to the sum of $M$ heat sources having Gaussian shape, where for $m = 1, 2, \dots, M$, the parameter $\epsilon_m$ controls the width of the source, $x_m \in \Omega$ is the center, and $\sigma_m(t) \geq 0$, $t \in [0,T]$, is the intensity of the $m$th source. We note that when $\sigma_m(t) = 0$, for each $t \in [0,T]$, there is no source at $x_m$ during the simulation. The choice of expression (16) provides some computational advantages that are explained in the following sections; however, it allows the approximation of general source shapes as a consequence of the well-known properties of the Gaussian radial basis functions [27]; see Chapters 10 and 11, a choice proposed also for other applications [28–30]. However, when $G$ is given by (14), the integrand function can be written as the sum of terms of the form $Ce^{-(a\xi^2+b\xi+c)}$, for suitable choices of the coefficients $C$, $a > 0$, $b$, and $c$. For these functions, we can consider the following formula:

$$\begin{aligned} \int_0^L e^{-(a\xi^2+b\xi+c)} d\xi &= \frac{1}{2}\sqrt{\frac{\pi}{a}} e^{\frac{b^2}{4a}-c} \\ &\left( \operatorname{erf}\left( \frac{2aL+b}{2\sqrt{a}} \right) - \operatorname{erf}\left( \frac{b}{2\sqrt{a}} \right) \right), \quad a > 0, \end{aligned} \tag{18}$$

where erf is the error function; see [24] Chapter 7 for details.

For simplicity, in the description of the numerical scheme, we fix the ideas on the generic $m$th source; that is, we assume that the source term function in (1) is of the following form:

$$f(x,t) = \frac{1}{\sqrt{2\pi}} \sigma_m(t) f_m(x) \tag{19}$$

Note that this is not a restrictive assumption because all the operators involved in the following discussion are linear. In this case, the values of the parameters $C$ and $a$ are equal for all the five exponential terms in (14) and are given by the following:

$$C = \frac{\sigma_m(t)}{2\pi\sqrt{2\alpha(t-\tau)}}, \quad a = \frac{1}{\mathcal{T}} + \epsilon_m^2.$$

Moreover, it is easy to prove that the values of coefficients $b$ and $c$ for the exponential terms in the product between (17) and (14) are given, for $n = 0, \dots, N$, by the following:

$$b_1 = -\frac{2x}{\mathcal{T}} - 2x_m\epsilon_m^2 \tag{20}$$

$$b_{h,n} = \begin{cases} \frac{4nL+4L-2x}{\mathcal{T}} - 2x_m\epsilon_m^2, & h = 2, \\ \frac{-4nL-4L+2x}{\mathcal{T}} - 2x_m\epsilon_m^2, & h = 3, \\ \frac{-4nL-4L-2x}{\mathcal{T}} - 2x_m\epsilon_m^2, & h = 4, \\ \frac{4nL+2x}{\mathcal{T}} - 2x_m\epsilon_m^2, & h = 5, \end{cases} \tag{21}$$

$$c_1 = \frac{x^2}{\mathcal{T}} + \epsilon_m^2 x_m^2 \tag{22}$$

$$c_{h,n} = \begin{cases} \frac{4n^2L^2+8nL^2-4nLx+4L^2-4Lx+x^2}{\mathcal{T}} + \epsilon_m^2 x_m^2, & h = 2, \\ \frac{4n^2L^2+8nL^2-4nLx+4L^2-4Lx+x^2}{\mathcal{T}} + \epsilon_m^2 x_m^2, & h = 3, \\ \frac{4n^2L^2+8nL^2+4nLx+4L^2+4Lx+x^2}{\mathcal{T}} + \epsilon_m^2 x_m^2, & h = 4, \\ \frac{4n^2L^2+4nLx+4L^2+x^2}{\mathcal{T}} + \epsilon_m^2 x_m^2, & h = 5. \end{cases} \tag{23}$$

Now, for each term, we can perform some simplifications that lead to the following integral:

$$\int_0^t \frac{\sigma_m(\tau)}{\sqrt{2\pi}} \cdot P(a,b,c) d\tau \tag{24}$$

where we define $P(a,b,c)$ as follows:

$$\begin{aligned} P(a,b,c) &= \frac{e^{\frac{b_1^2}{4a}-c_1}}{\sqrt{1+\epsilon_m^2\mathcal{T}}} \left( \operatorname{erf}\left( \frac{2aL+b_1}{2\sqrt{a}} \right) - \operatorname{erf}\left( \frac{b_1}{2\sqrt{a}} \right) \right) \\ &+ \sum_{h=2}^{5} \sum_{n=0}^{N} \left( \frac{e^{\frac{b_{h,n}^2}{4a}-c_{h,n}}}{\sqrt{1+\epsilon_m^2\mathcal{T}}} \left( \operatorname{erf}\left( \frac{2aL+b_{h,n}}{2\sqrt{a}} \right) - \operatorname{erf}\left( \frac{b_{h,n}}{2\sqrt{a}} \right) \right) \right). \end{aligned} \tag{25}$$

Integral (24) can be easily approximated with the trapezoidal rule, since it no longer has a singularity at $t = \tau$.

### 2.3 | Three-Dimensional Problem

We consider the three-dimensional problem that generalizes problem (1). Let $B = [0, L_1] \times [0, L_2] \times [0, L_3] \subset \mathbb{R}^3$, $L_1 > 0, L_2 > 0, L_3 > 0$ be the spatial domain and let $\mathbf{x} = (x_1, x_2, x_3)^t \in B$. We are looking for the solution of the following problem:

$$\begin{cases} \frac{\partial u}{\partial t}(\mathbf{x}, t) - \alpha \Delta u(\mathbf{x}, t) = \phi(\mathbf{x}, t), & \mathbf{x} \in B,\ t \in [0, T], \\ \frac{\partial u}{\partial \hat{n}}(\mathbf{x}, t) = 0, & \mathbf{x} \in \partial B,\ t \in [0, T], \\ u(\mathbf{x}, 0) = U_0(\mathbf{x}), & \mathbf{x} \in B, \end{cases} \tag{26}$$

where $\Delta$ is the Laplacian operator in the three-dimensional Cartesian coordinate system, that is, $\Delta u = \frac{\partial^2 u}{\partial x^2} + \frac{\partial^2 u}{\partial y^2} + \frac{\partial^2 u}{\partial z^2}$, and $\hat{n}(\mathbf{x})$ represents the unit outward normal at $\mathbf{x} \in \partial B$.

Given $\boldsymbol{\xi} = (\xi_1, \xi_2, \xi_3)^t \in B$, $\tau < t$, we consider the Green function $\Gamma$, solution of the problem

$$\begin{cases} \frac{\partial \Gamma}{\partial t}(\mathbf{x}, t; \boldsymbol{\xi}, \tau) - \alpha \Delta \Gamma(\mathbf{x}, t; \boldsymbol{\xi}, \tau) \\ \qquad = \delta(\mathbf{x} - \boldsymbol{\xi}) \delta(t - \tau), & \mathbf{x} \in B,\ t \in [0, T], \\ \frac{\partial \Gamma}{\partial \hat{n}}(\mathbf{x}, t; \boldsymbol{\xi}, \tau) = 0, & \mathbf{x} \in \partial B,\ t \in [0, T], \\ \Gamma(\mathbf{x}, 0; \boldsymbol{\xi}, \tau) = 0, & \mathbf{x} \in B. \end{cases} \tag{27}$$

From the Cartesian symmetry of $B$, we can easily see that $\Gamma$ can be expressed in terms of the Green function of the one-dimensional problem, that is,

$$\Gamma(\mathbf{x}, t; \boldsymbol{\xi}, \tau) = G(x_1, t; \xi_1, \tau) G(x_2, t; \xi_2, \tau) G(x_3, t; \xi_3, \tau); \tag{28}$$

see [21] for details. As in the one-dimensional problem, we assume that the source function $\phi(\mathbf{x}, t)$ in problem (26) has the following form:

$$\phi(\mathbf{x}, t) = \frac{1}{\sqrt{2\pi}} \sum_{m=1}^{M} \sigma_m(t) \prod_{i=1}^{3} f_{m,i}(x_i) \tag{29}$$

where

$$f_{m,i}(y) = e^{-\epsilon_{m,i}^2 (y - x_{m,i})^2}, \qquad i = 1, 2, 3; \quad m = 1, 2, \dots, M,$$

and $\tilde{\mathbf{x}}_m = (x_{m,1}, x_{m,2}, x_{m,3})^t \in B$ denotes the position of an heat source having intensity $\sigma_m(t)$. As in the one-dimensional problem, the solution $u(\mathbf{x}, t; \boldsymbol{\sigma}, U_0)$ of problem (26) can be expressed as follows:

$$\begin{aligned} u(\mathbf{x}, t; \boldsymbol{\sigma}, U_0) = & \int_B \Gamma(\mathbf{x}, t; \boldsymbol{\xi}, 0) U_0(\boldsymbol{\xi}) d\boldsymbol{\xi} \\ & + \int_0^t \left( \int_B \Gamma(\mathbf{x}, t; \boldsymbol{\xi}, \tau) \phi(\boldsymbol{\xi}, \tau) d\boldsymbol{\xi} \right) d\tau. \end{aligned} \tag{30}$$

We analyze the second addendum in (30), and for $0 \le \tau \le t$, we have that

$$\begin{aligned} & \int_B \Gamma(\mathbf{x}, t; \boldsymbol{\xi}, \tau) \phi(\boldsymbol{\xi}, \tau) d\boldsymbol{\xi} \\ & = \sum_{m=1}^{M} \frac{\sigma_m(\tau)}{\sqrt{2\pi}} \prod_{i=1}^{3} \int_0^{L_i} G(x_i, t; \xi_i, \tau) f_{m,i}(\xi_i) d\xi_i. \end{aligned} \tag{31}$$

Each one of the integrals

$$\int_0^{L_i} G(x_i, t; \xi_i, \tau) f_{m,i}(\xi_i) d\xi_i \qquad i = 1, 2, 3$$

can be evaluated as shown in Section 2.2, thus enabling the numerical approximation of $u(\mathbf{x}, t; \boldsymbol{\sigma}, U_0)$ given in (30).

## 3 | The Inverse Problem

We consider an inverse source problem associated to problem (26), where the source function is completely defined from vector $\boldsymbol{\sigma}(t) = (\sigma_1(t), \sigma_2(t), \dots, \sigma_M(t))^T$. In particular, the following problem is studied.

**Problem 1.** Given $\mu_i(t_j)$, $i = 1, 2, \dots, I$, $j = 1, \dots, J + 1$, the temperature measurements at known points $\mathbf{x}_i \in B$, $i = 1, 2, \dots, I$, at times $t_j$, $j = 1, \dots, J + 1$, compute the source intensities $\boldsymbol{\sigma}(t_j)$ such that $u(\mathbf{x}_i, t_j; \boldsymbol{\sigma}, U_0) = \mu_i(t_j)$, $i = 1, 2, \dots, I$, $j = 1, \dots, J + 1$.

The integral formulation (30) for the solution of problem (26) allows us to formulate Problem 1 as an integral equation for the source intensity functions $\boldsymbol{\sigma}(t)$. In particular, with the notation introduced in the previous section, we have the following:

$$\begin{aligned} & u(\mathbf{x}_i, t_j; \boldsymbol{\sigma}, U_0) - \int_B \Gamma(\mathbf{x}_i, t_j; \boldsymbol{\xi}, 0) U_0(\boldsymbol{\xi}) d\boldsymbol{\xi} \\ & = \int_0^{t_j} \left( \int_B \Gamma(\mathbf{x}_i, t_j; \boldsymbol{\xi}, \tau) \phi(\boldsymbol{\xi}, \tau) d\boldsymbol{\xi} \right) d\tau, \end{aligned} \tag{32}$$

where the innermost integral at the right-hand side is evaluated by formula (31). Hence, the right-hand side of (32) can be rewritten as follows:

$$\sum_{m=1}^{M} \int_0^{t_j} \sigma_m(\tau) \Phi_m(\mathbf{x}, t_j; \tau) d\tau,$$

where the functions $\Phi_m(\mathbf{x}, t_j; \tau)$ are obtained by applying formulas developed in Section 2.2 to analytically compute the corresponding integrals in (31); instead, the time integrals are numerically approximated by the trapezoidal quadrature rule. Moreover, we can notice that the left-hand side of (32) is a known term for all $\mathbf{x}_i$, $i = 1, \dots, I$ and $t_j$, $j = 1, \dots, J + 1$. Now, the procedure to construct the linear system of the form $A\boldsymbol{\sigma} = \mathbf{b}$ from the modified version of Equation (32) is presented.

We define the vector $\boldsymbol{\sigma} = (\boldsymbol{\sigma}_1^t, \dots, \boldsymbol{\sigma}_M^t)^t \in \mathbb{R}^{M(J+1)}$, where the generic vector $\boldsymbol{\sigma}_m = (\sigma_m(t_1), \dots, \sigma_m(t_{J+1}))^t \in \mathbb{R}^{J+1}$ contains the values of the $m$-th source intensity at different observation times. The vector $\mathbf{b} = (\mathbf{b}_1^t, \dots, \mathbf{b}_{J+1}^t)^t \in \mathbb{R}^{I(J+1)}$ is given by the

**TABLE 1** | Numerical experiments proposed.

| Case studied | Source configuration | Active sources |
|---|---|---|
| Case 1 | $2 \times 2$ grid | One active source |
| Case 2 | $2 \times 2$ grid | Two active sources |
| Case 3 | $3 \times 3$ grid | One active source |

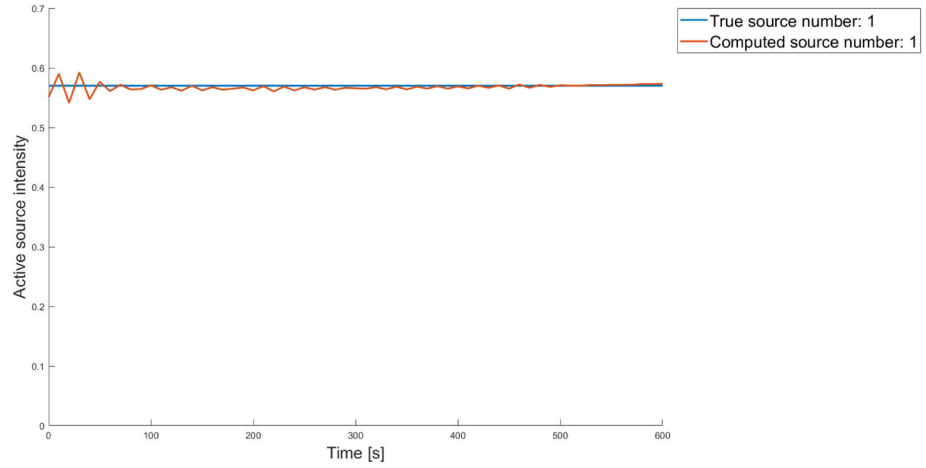


Intensity value.

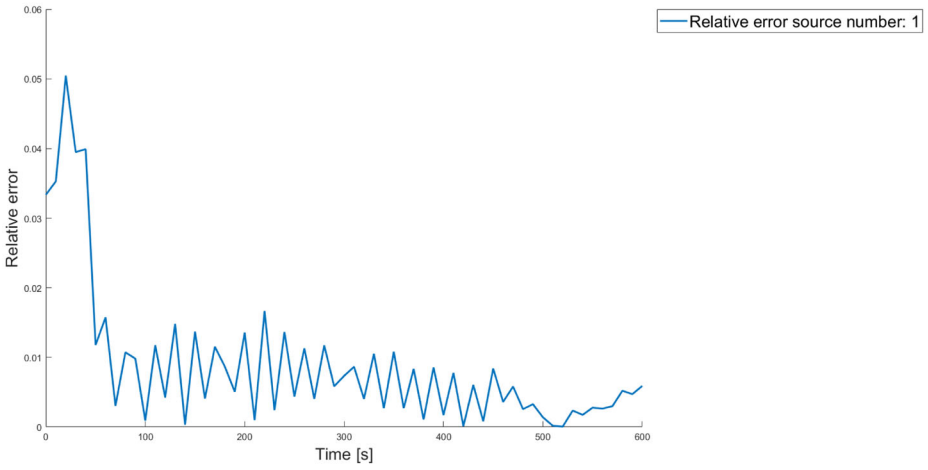


Relative error.

**FIGURE 1** | Case 1: Plot of the active source intensity (top) and its relative error over time (bottom). [Colour figure can be viewed at wileyonlinelibrary.com]

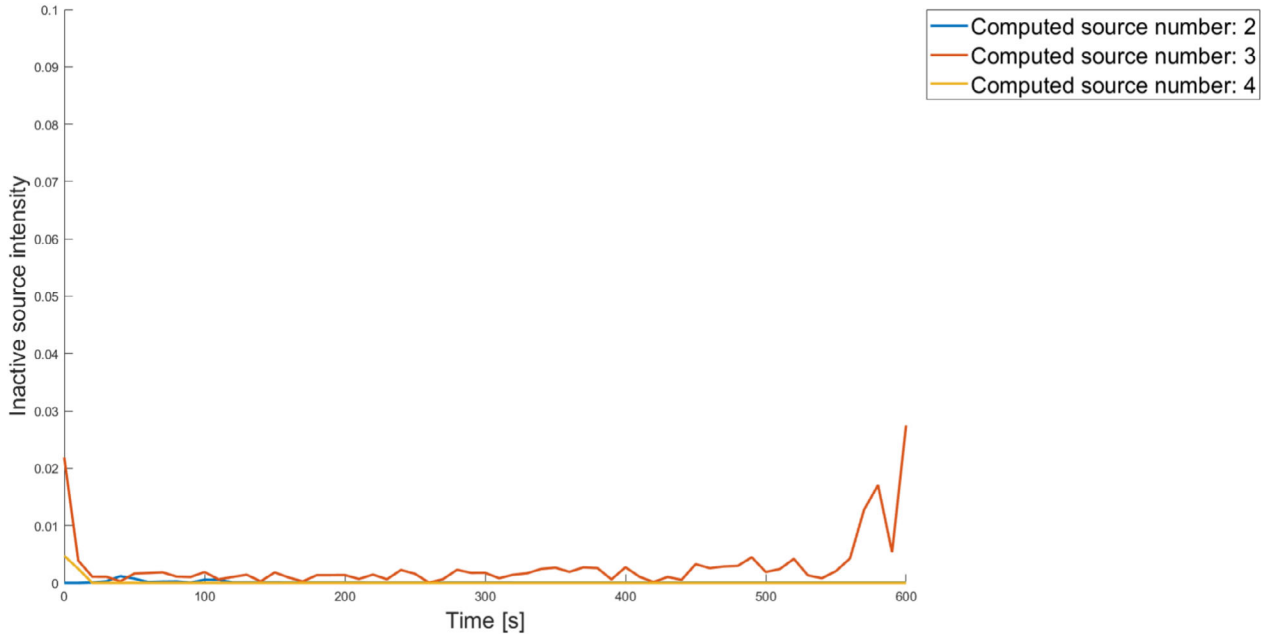


**FIGURE 2** | Case 1: Plot of the inactive sources intensity over time. [Colour figure can be viewed at wileyonlinelibrary.com]

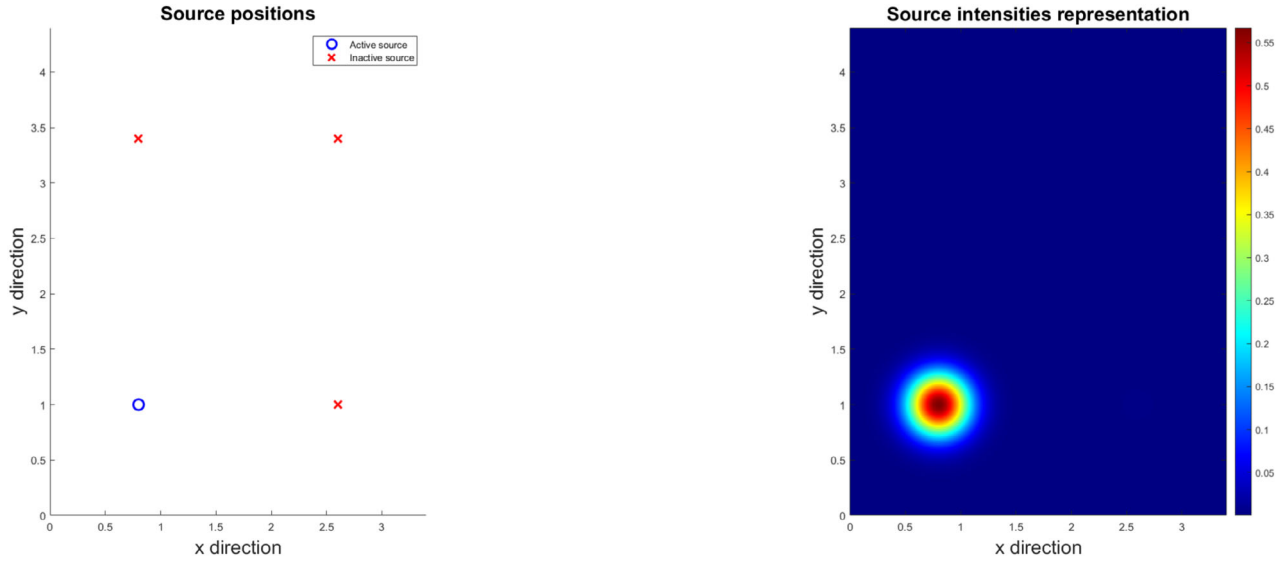


**FIGURE 3** | Case 1: Sources grid positions (left) and visual representation of the computed heat source intensities (right). [Colour figure can be viewed at wileyonlinelibrary.com]

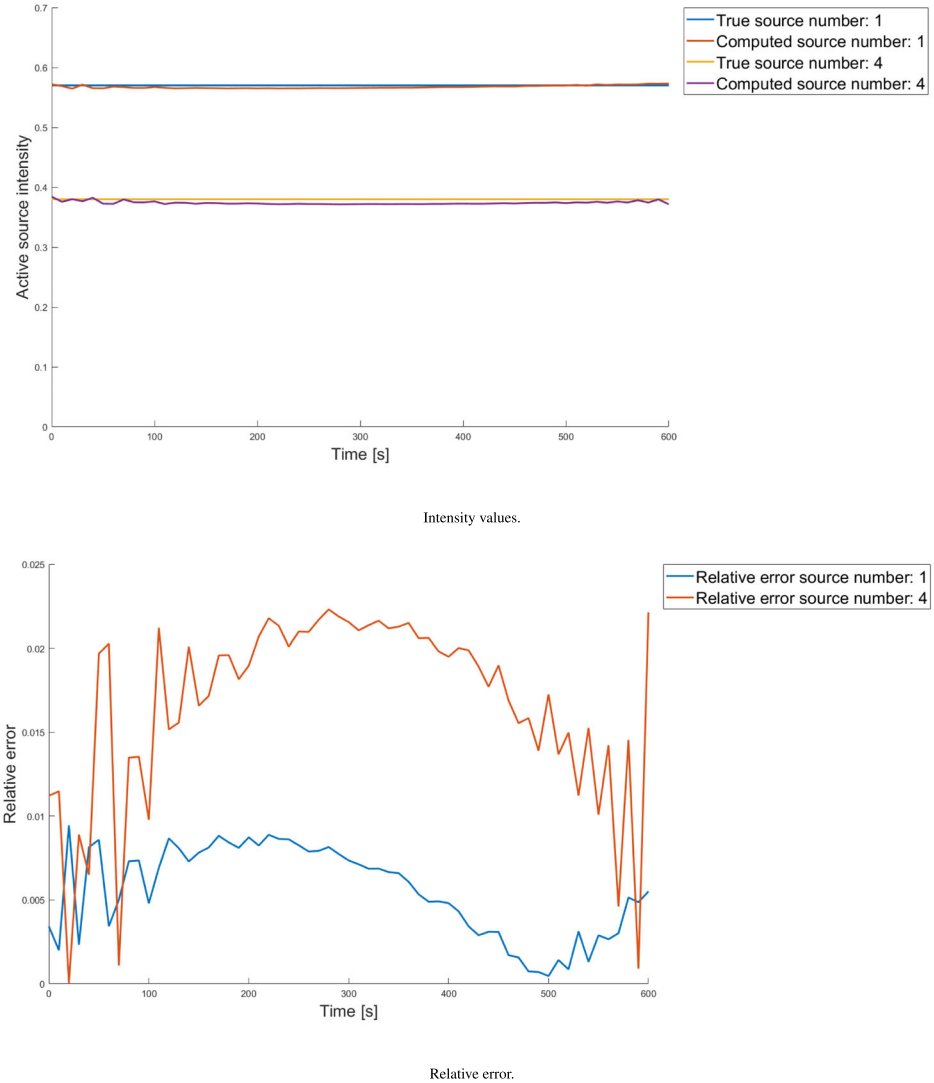


**FIGURE 4** | Case 2: Plot of the active source intensities (top) and their relative error over time (bottom). [Colour figure can be viewed at wileyonlinelibrary.com]

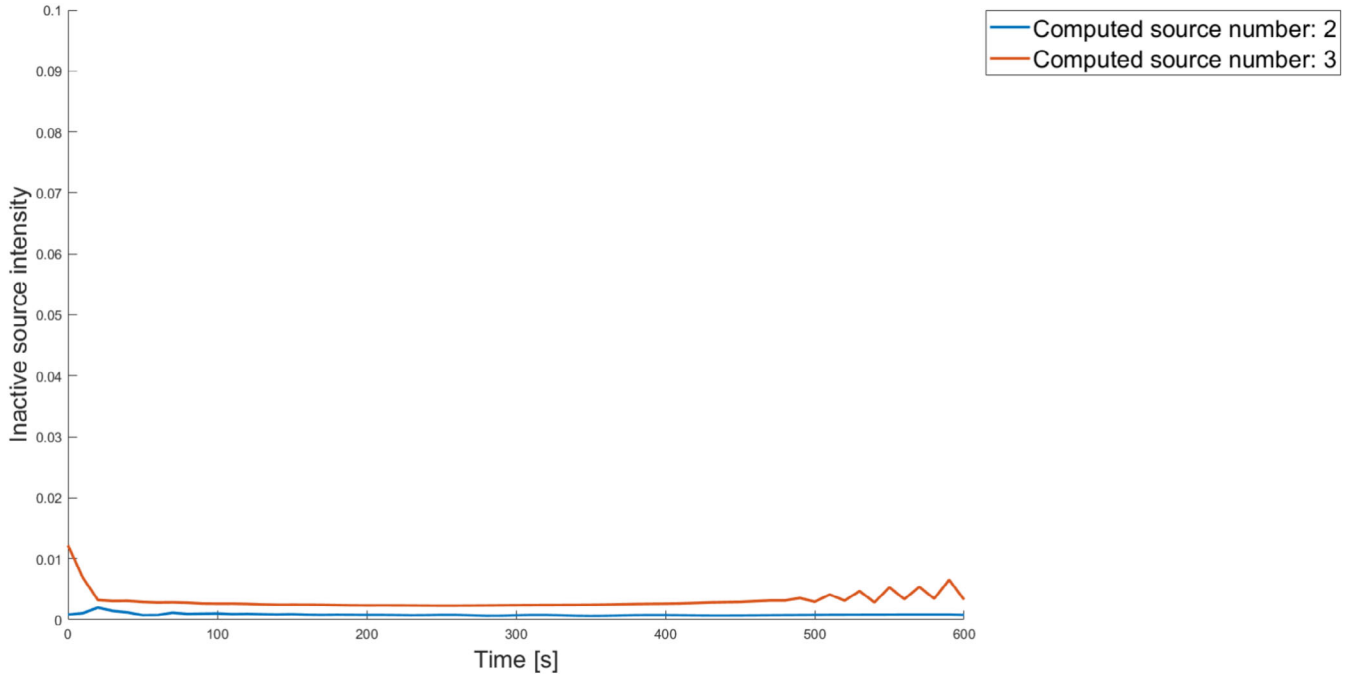


**FIGURE 5** | Case 2: Plot of the inactive sources intensity over time. [Colour figure can be viewed at wileyonlinelibrary.com]

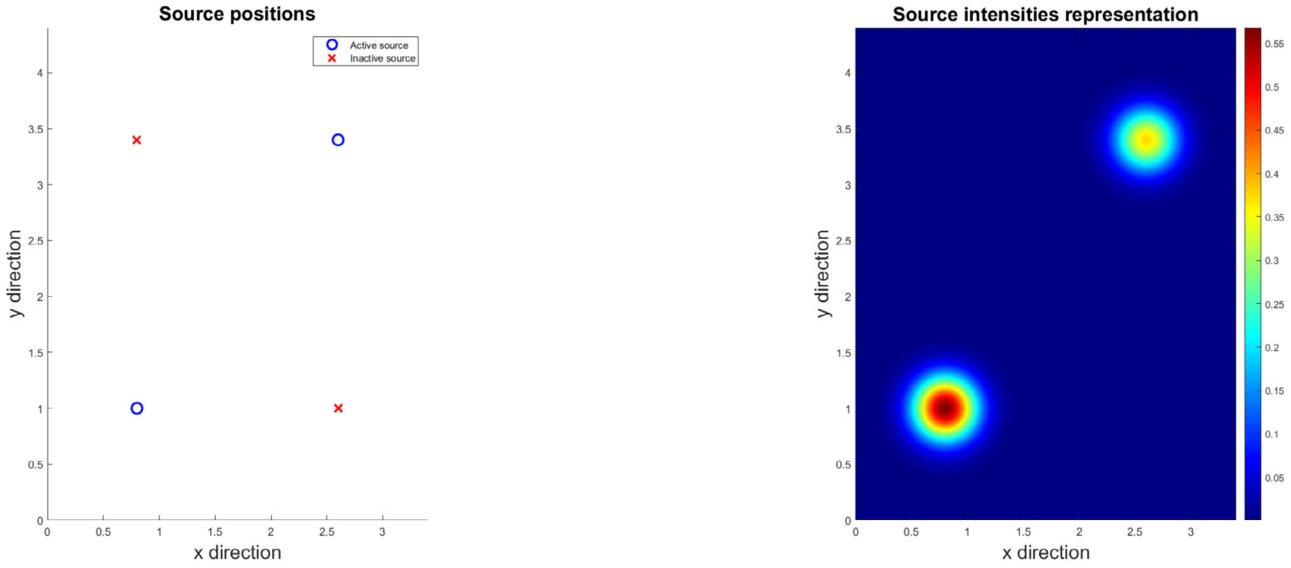


**FIGURE 6** | Case 2: Sources grid positions (left) and visual representation of the computed heat source intensities (right). [Colour figure can be viewed at wileyonlinelibrary.com]

concatenation of $J+1$ vectors $\mathbf{b}_j \in \mathbb{R}^I$, $j = 1, \ldots, J+1$, which have the $i$th component equal to

$$(\mathbf{b}_j)_i = u(\mathbf{x}_i, t_j; \boldsymbol{\sigma}, U_0) - \int_B \Gamma(\mathbf{x}_i, t_j; \boldsymbol{\xi}, 0) U_0(\boldsymbol{\xi}) d\boldsymbol{\xi}, i = 1, \ldots, I. \tag{33}$$

Thus, the matrix $A$ can be defined as $A = (A_1 | \ldots | A_M)$, where the generic matrix $A_m \in \mathbb{R}^{JI \times J+1}$ is composed of $J$ block matrices $A_{m,j} \in \mathbb{R}^{I \times J+1}$ having components equal to

$$A_{m,j}(i, \hat{j}) = \begin{cases} \omega_{\hat{j}} \Phi_m(\mathbf{x}_i, t_j, \tau_{\hat{j}}) & \text{if } \hat{j} \le j+1, \\ 0 & \text{if } \hat{j} > j+1, \end{cases} \tag{34}$$

where $\omega_{\hat{j}}$ are the weights assigned to the trapezoidal quadrature formula.

The linear system $A\boldsymbol{\sigma} = \mathbf{b}$ is not directly solved since it is ill-conditioned and also because we need to enforce a solution $\boldsymbol{\sigma}$ with nonnegative components. For these reasons, we use the Tikhonov regularization procedure, and in the corresponding minimization problem, we consider the bound constraint; that is, we solve the following problem:

$$\begin{aligned} &\text{minimize} \quad \tfrac{1}{2}\left(\|A\boldsymbol{\sigma} - \mathbf{b}\|_2^2 + \lambda \|\boldsymbol{\sigma}\|_2^2\right), \\ &\text{subject to} \quad \boldsymbol{\sigma} \ge 0 \end{aligned} \tag{35}$$

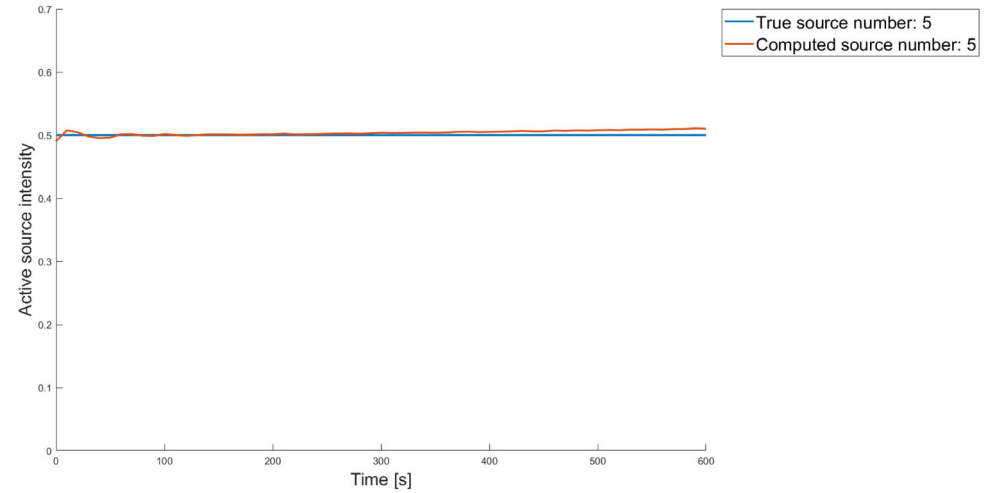


Intensity value.

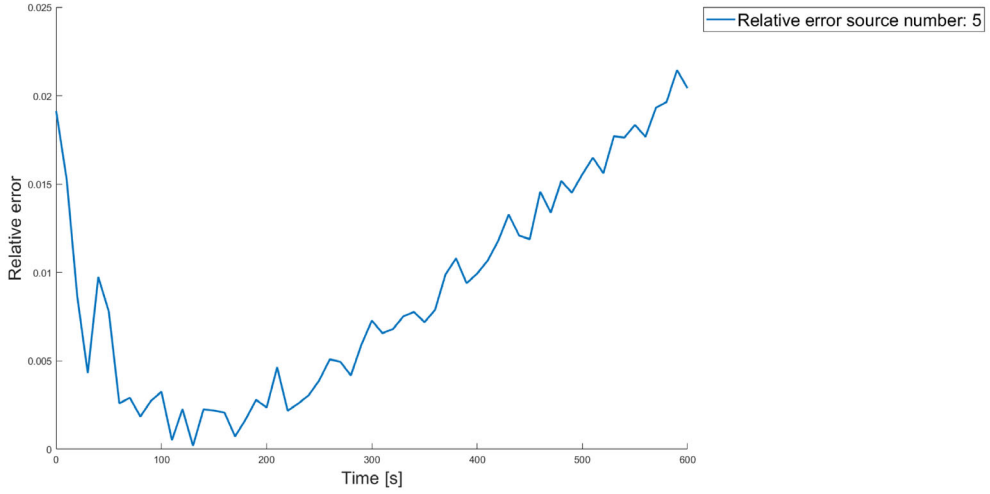


Relative error.

**FIGURE 7** | Case 3: Plot of the active source intensity (top) and its relative error over time (bottom). [Colour figure can be viewed at wileyonlinelibrary.com]

where $\lambda$ is the Tikhonov regularization parameter; see [10] for details on this regularization method.

## 4 | Numerical Results

We present the results obtained from some numerical experiments designed to assess the effectiveness of the proposed method. In these experiments, we simulate a closed room with fixed sensors near the ceiling to measure the temperature generated from different source configurations.

The closed room is represented by the spatial domain $B = [0, L_1] \times [0, L_2] \times [0, L_3]$, where the maximum length are $L_1 = 3.4$ m, $L_2 = 4.4$ m, and $L_3 = 2.7$ m, where $m$ denotes meters. The thermal diffusivity $\alpha$ is $2.17 \cdot 10^{-5} \frac{\mathrm{m}^2}{\mathrm{s}}$, where s denotes seconds. All the simulations are made on a time interval $[0, T]$, with $T = 600$ s. We suppose to have a uniform grid of $4 \times 5$ thermal detectors, at a height $z = 2.45$ m; the grid is placed on a hypothetical rectangle that is 0.5m away from the walls. The grid consists of four detectors along the $x$-direction and 5 points along the $y$-direction.

The numerical solution of the initial-boundary value problem (26) is computed by the finite difference scheme with a uniform space grid having $N_x = 17$, $N_y = 22$, and $N_z = 21$ nodes in the $x$, $y$, and $z$ directions, respectively. The simulation time interval has been partitioned in $N_t = 61$ time steps, resulting with $\Delta t = 10$ s, so the Courant–Friedrichs–Lewy (CFL) condition for the three-dimensional heat equation is satisfied [31].

Two different source configurations are considered. The first configuration is a $2 \times 2$ grid, and the second configuration is a $3 \times 3$ grid, both grids placed at a fixed height of $z = 0.5$ m. We note that this choice to place all sources on the same horizontal plane is motivated by a specific application context, namely, indoor human localization in public environments. In such settings, individuals typically occupy a relatively narrow vertical range

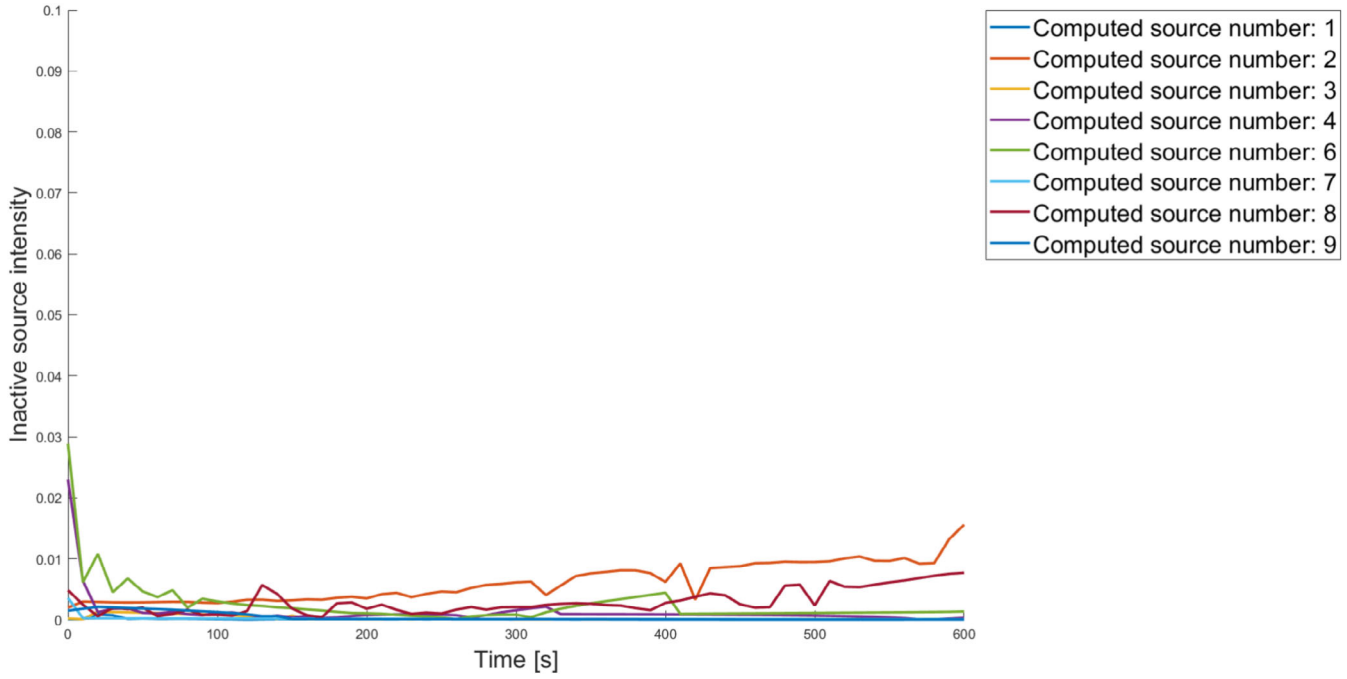


**FIGURE 8** | Case 3: Plot of the inactive sources intensity over time. [Colour figure can be viewed at wileyonlinelibrary.com]

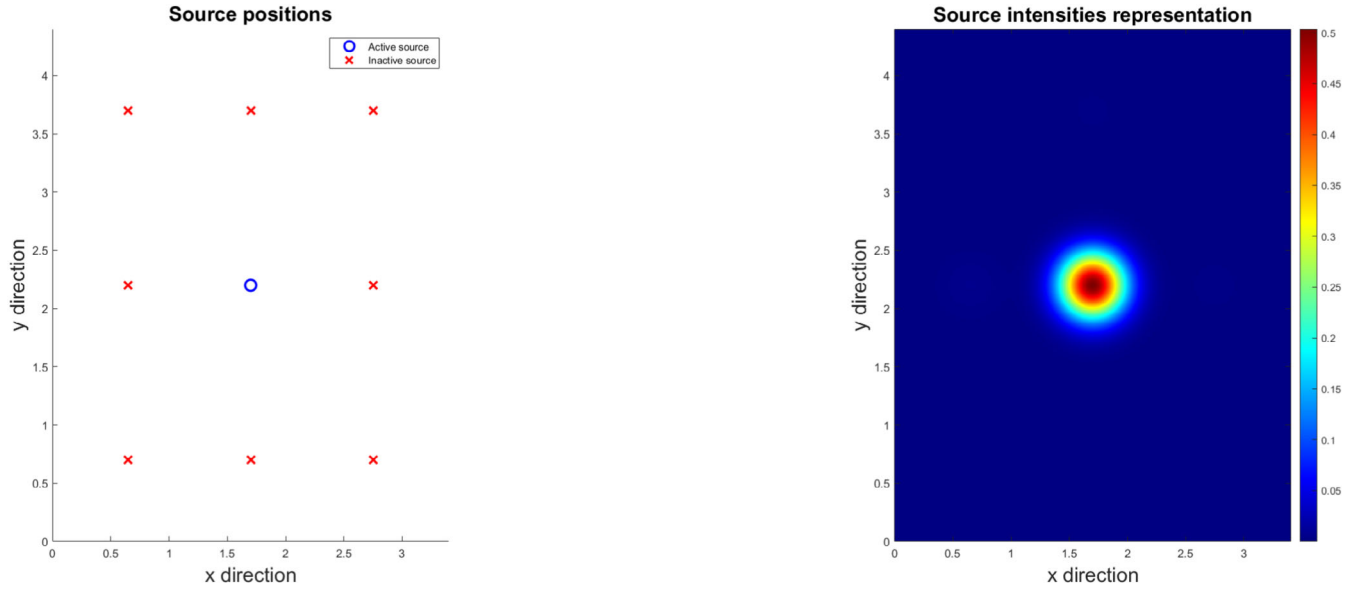


**FIGURE 9** | Case 3: Sources grid positions (left) and visual representation of the computed heat source intensities (right). [Colour figure can be viewed at wileyonlinelibrary.com]

(e.g., standing or sitting at a common average height), which justifies the assumption of coplanar sources. This assumption also serves as a stabilization strategy in the inverse problem. While extending the model to allow sources distributed across multiple planes is theoretically feasible, it would introduce additional degrees of freedom and complexities that require different configuration in the problem data. Table 1 provides a summary of such configurations. The numerical solution of problem (35) is computed by a Newton method modified to deal with bound constraints [32]; in particular, for this method, we have used the MatLab provided by function lsqlin [33]. In problem (35), we have chosen the regularization parameter $\lambda = 5 \cdot 10^{-5}$ through a process of trial and error, with the objective of finding the best trade-off between stability and reconstruction accuracy. However, from results not reported in this paper, we have that slight different regularization parameters provide similar source positions but with slightly different intensity. In the practical application of the method, an automatic selection of the regularization parameter should be done, for example, by using the Morozov discrepancy principle [34]. Figures 1–9 show the behavior over time of the computed source intensity versus the actual source intensity as well as the relative error over time. Moreover,

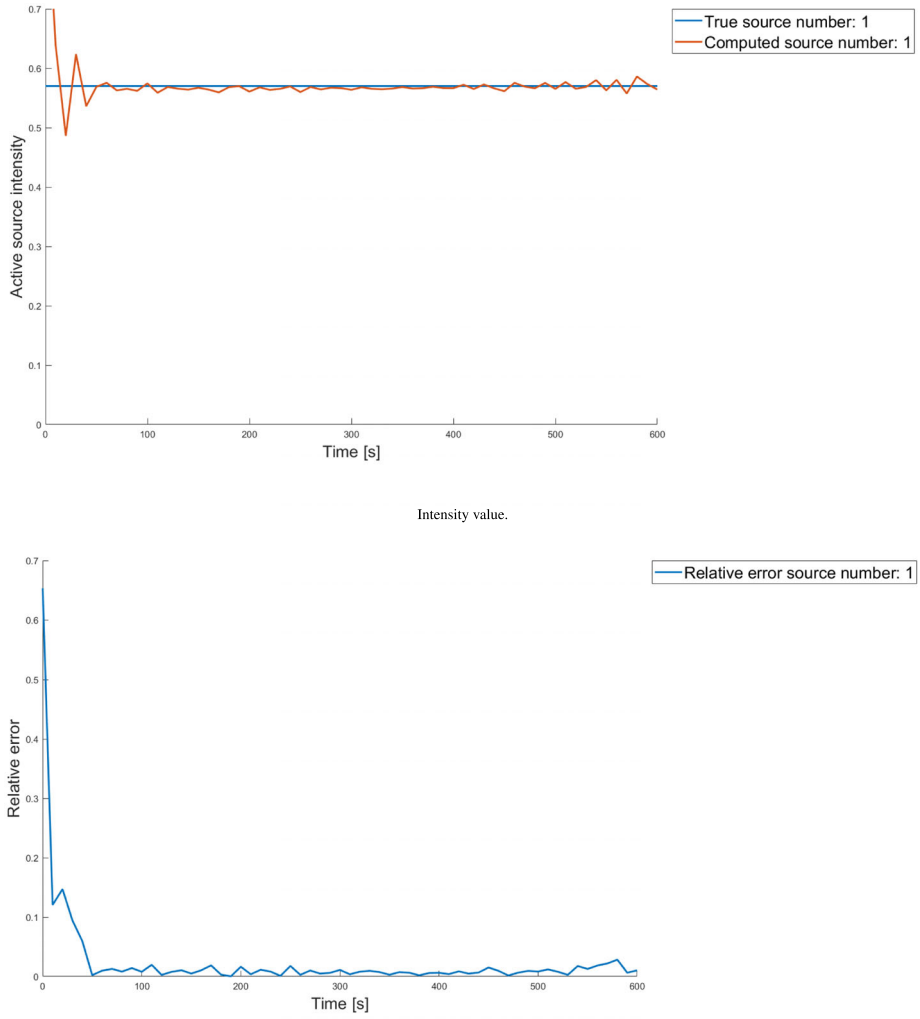


**FIGURE 10** | Plot of the active source intensity (top) and its relative error over time (bottom) with 1% noise added to the data. [Colour figure can be viewed at wileyonlinelibrary.com]

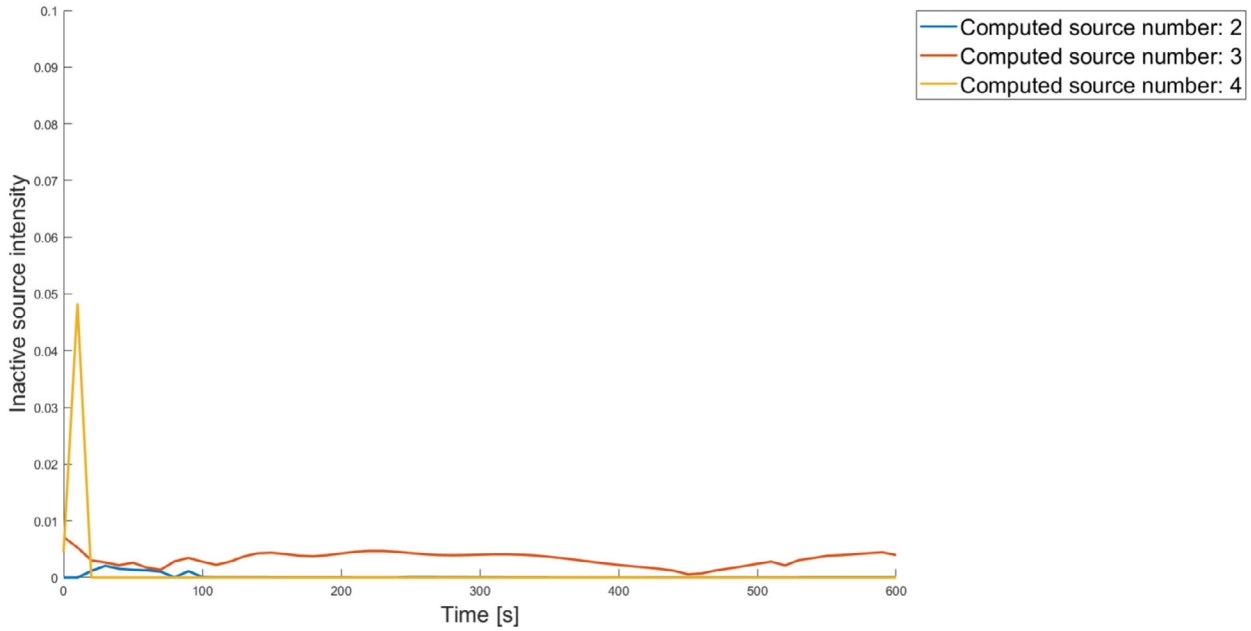


**FIGURE 11** | Plot of the inactive sources intensity over time with 1% noise added to the data. [Colour figure can be viewed at wileyonlinelibrary.com]

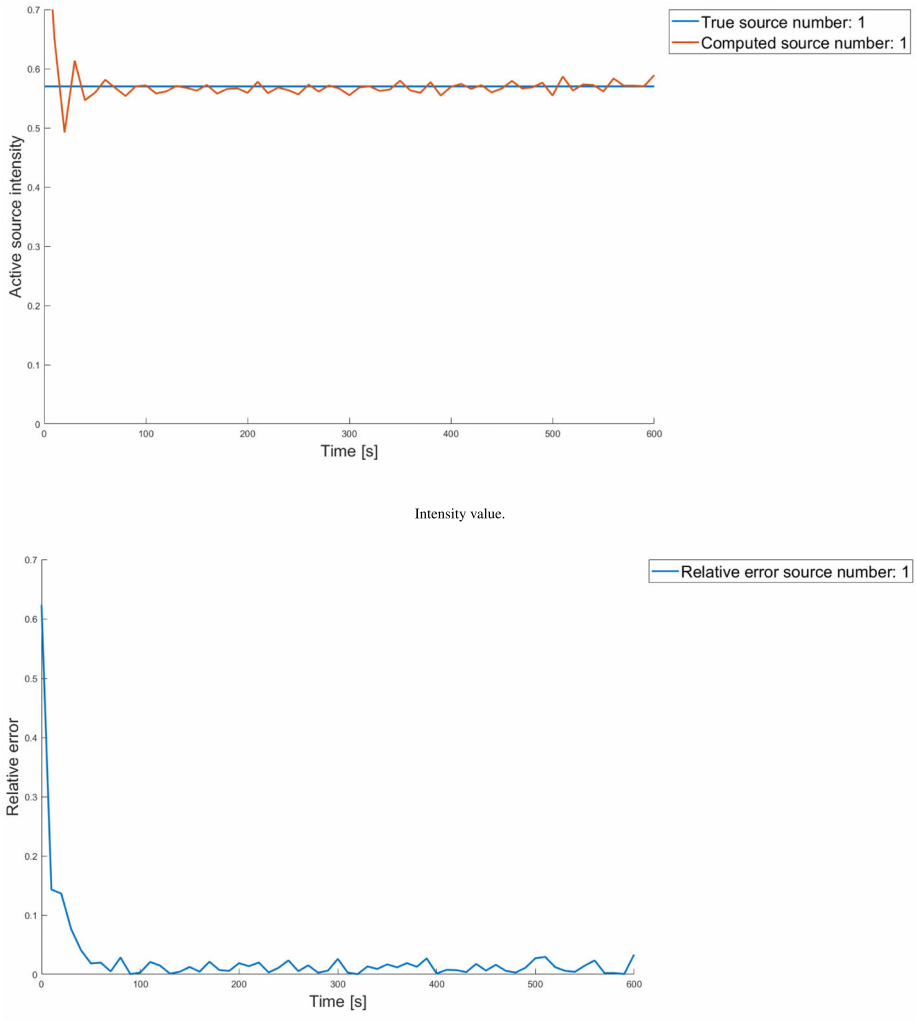


**FIGURE 12** | Plot of the active source intensity (top) and its relative error over time (bottom) with 2% noise added to the data. [Colour figure can be viewed at wileyonlinelibrary.com]

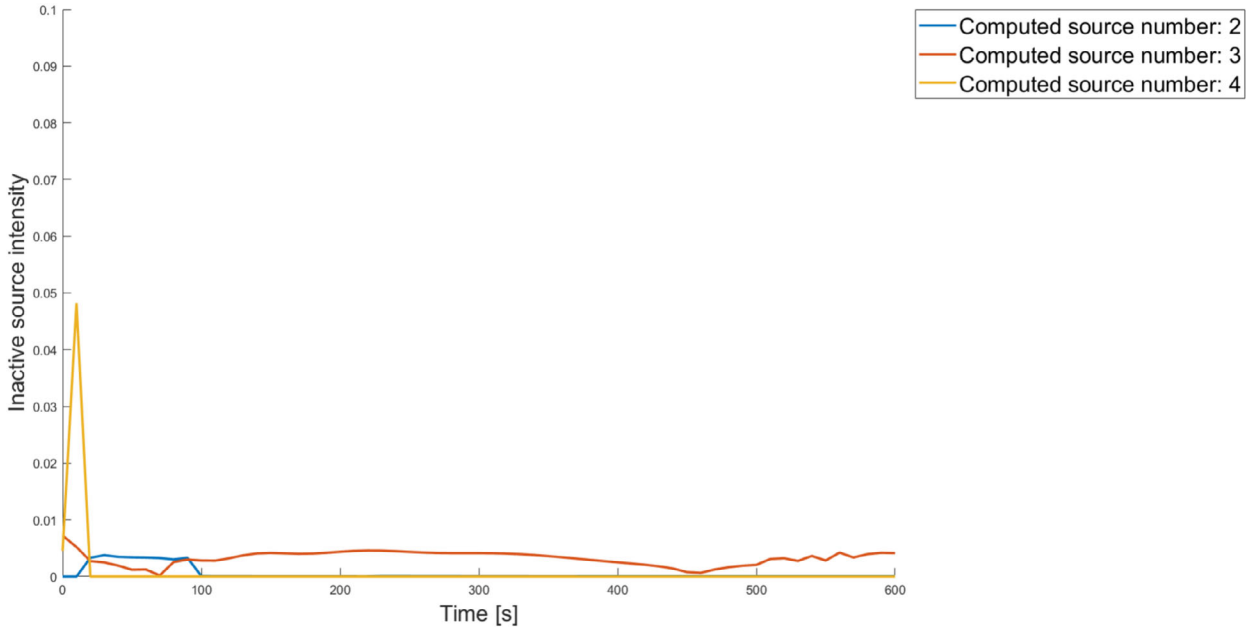


**FIGURE 13** | Plot of the inactive sources intensity over time with 2% noise added to the data. [Colour figure can be viewed at wileyonlinelibrary.com]

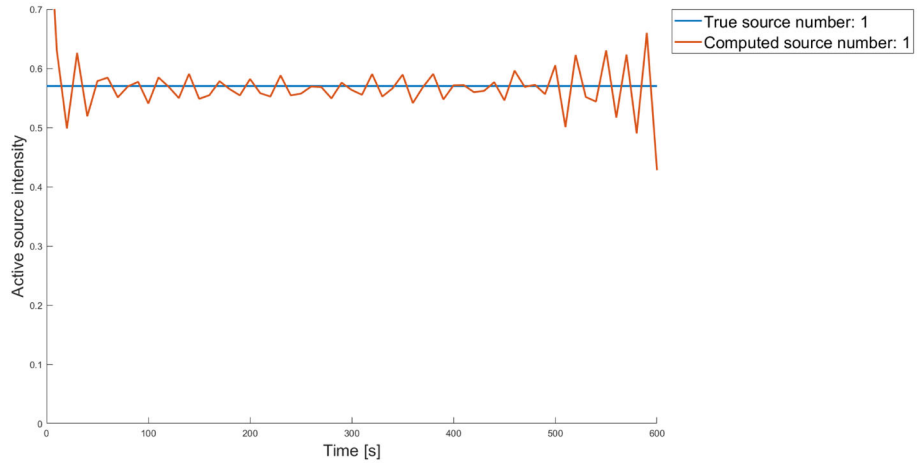


Intensity value.

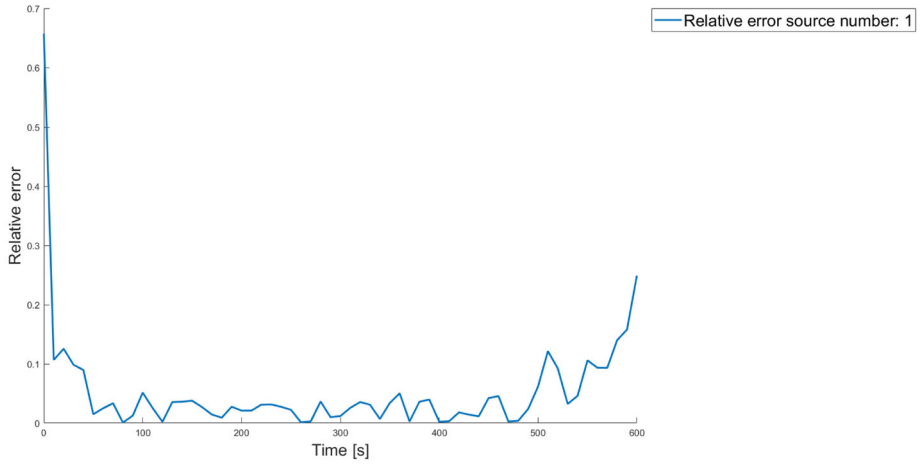


Relative error.

**FIGURE 14** | Plot of the active source intensity (top) and its relative error over time (bottom) with 5% noise added to the data. [Colour figure can be viewed at wileyonlinelibrary.com]

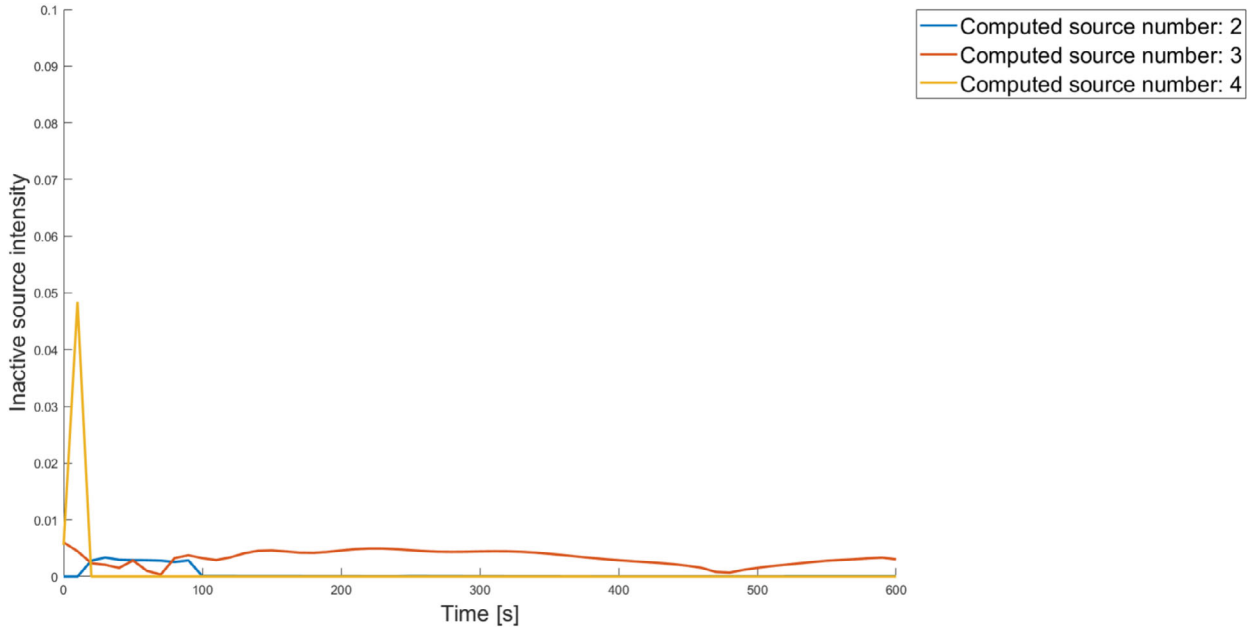


**FIGURE 15** | Plot of the inactive sources intensity over time with 5% noise added to the data. [Colour figure can be viewed at wileyonlinelibrary.com]

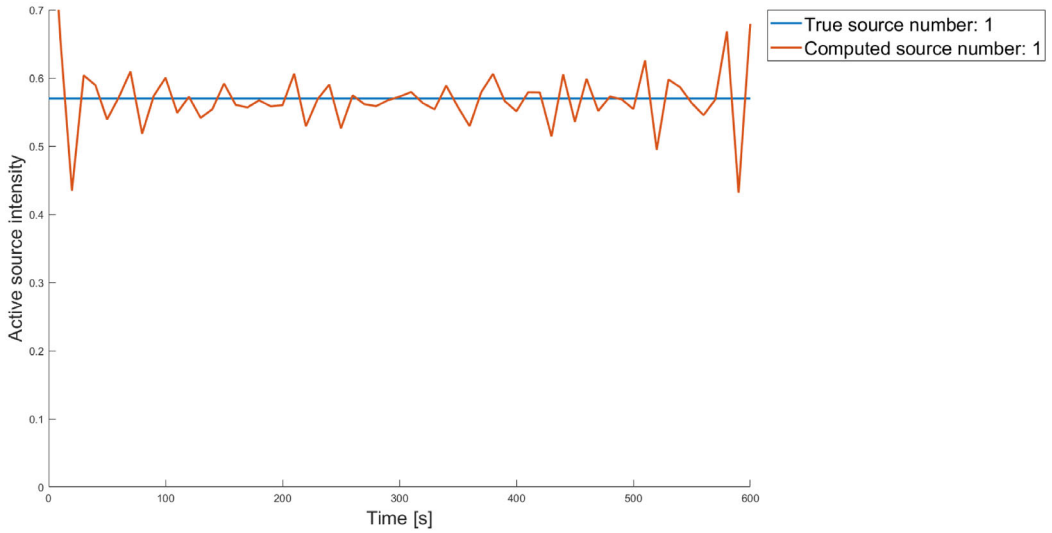


Intensity value.

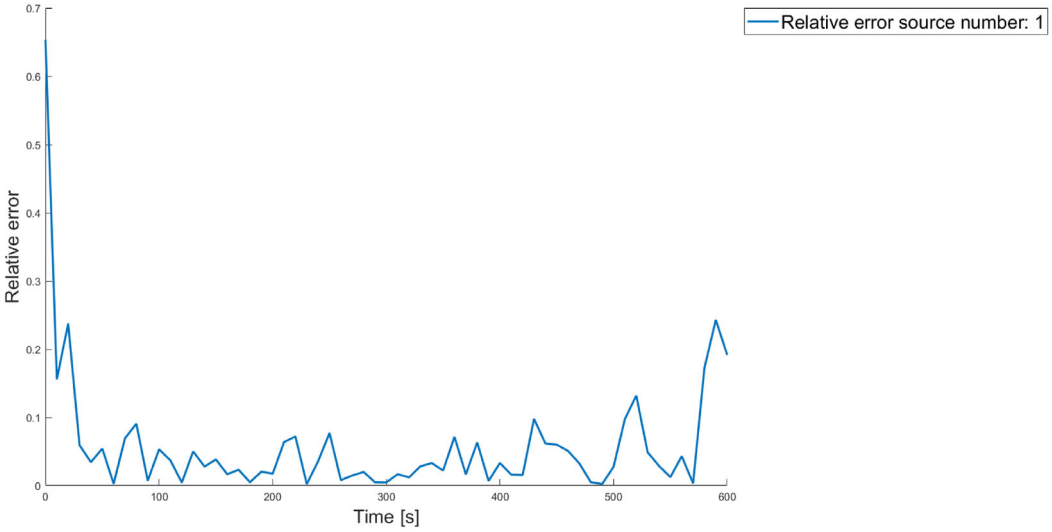


Relative error.

**FIGURE 16** | Plot of the active source intensity (top) and its relative error over time (bottom) with 10% noise added to the data. [Colour figure can be viewed at wileyonlinelibrary.com]

Figures 3, 6, and 9 give a visual representation of the reconstructed heat sources in a slice of the $xy$-plane at $z = 0.5$ m. In particular, Figures 1–3 refer to Case 1, Figures 4–6 refer to Case 2, and Figures 7–9 refer to Case 3.

Figure 1 compares the computed intensity of the active heat source with the actual active heat source intensity over time. In this first experiment, only a single heat source is active and the computed intensity closely follows the true value, indicating that the numerical method successfully captures the dynamics of the heat source, with a low and stable relative error produced. Figure 2 shows the computed intensity for the inactive sources where the true value is equal to zero. In Figure 3, a visual representation of the computed heat source intensities is shown in a slice of the $xy$-plane at a height of $z = 0.5$ m. This figure highlights the precise identification of the active source while inactive regions remain unaffected, further supporting the model's effectiveness in capturing the heat source in this scenario.

Figures 4–6 concern Case 2. Figure 4 compares the computed intensity values of two active heat sources with the actual active heat sources, again within the $2 \times 2$ grid configuration. In particular, Figure 4 illustrates how the numerical solution is able to differentiate between the two active sources, accurately tracking their respective intensities while keeping the respective relative errors low. At the same time, as shown in Figure 5, the inactive sources exhibit an intensity close to zero. While minor discrepancies between the computed and actual intensities are visible, the overall trend demonstrates the reliability of the numerical method in a more complex multisource scenario. In Figure 6, the corresponding heat source intensities are visualized, showing the successful localization of both the active sources.

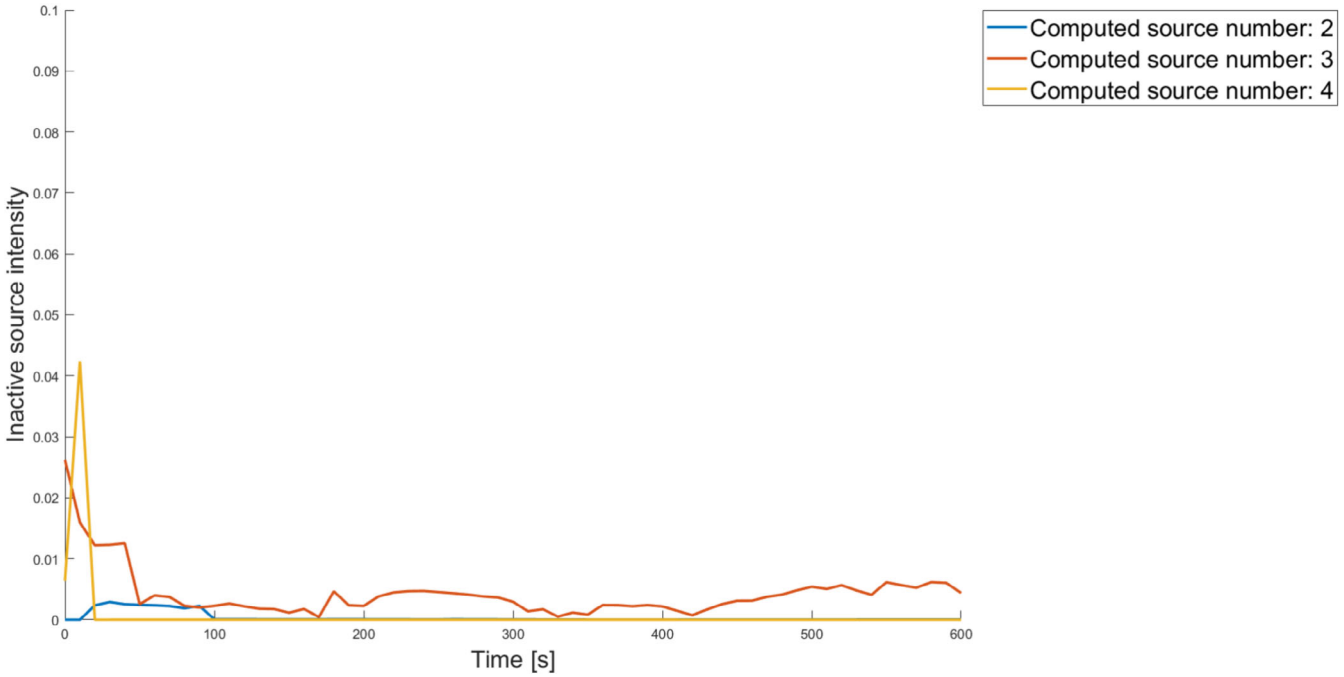


**FIGURE 17** | Plot of the inactive sources intensity over time with 10% noise added to the data. [Colour figure can be viewed at wileyonlinelibrary.com]

In Figure 7, the behavior of a single active source is presented in the case of a $3 \times 3$ grid configuration. The computed intensity is again in close agreement with the true intensity, with only minor variations visible as time progresses. This reinforces the model's consistency in identifying the heat source's behavior, even in a more complex grid setup. The same concept holds for the inactive sources, as shown in Figure 8. Similar to the previous experiments, Figure 9 visualizes the heat source intensity, confirming that the model accurately identifies the active source, while the inactive regions remain unaffected. In all the cases considered, the method successfully identifies the correct placement of the active sources, assigning a value close to zero to the inactive ones. So, these results highlight the robustness of the method for different source configurations and its ability to identify rapidly the active sources in the room (see Figures 1, 4, and 7). On the other hand, the diffusive nature of the heat equation seems to negatively influence the results obtained over long periods. This last point has to be analyzed in a future study of the proposed method. Figures 10–17 highlight the behavior of the proposed method with an added noise of 1%, 2%, 5%, and 10%, applied to the set up of Case 1. It should be noted that a dedicated study to find an optimal value of the $\lambda$ parameter would yield more stable results; however, this is outside the scope of the presented work.

Figure 10 compares the computed intensity of the active heat source with the actual active heat source intensity over time. The computed intensity closely follows the true value, indicating that the numerical method successfully captures the dynamics of the heat source, with a low and stable relative error produced. Figure 11 shows the computed intensity for the inactive sources where the true value is equal to zero. We can conclude that the noise level of 1% does not have notable negative effects on the numerical method proposed. The comparison proposed in Figures 12 and 13 between the computed heat source intensities with a noise level of 2% of the temperature data shows the ability of the numerical method of correctly identifying the heat source position and intensity, while keeping a low relative error.

Figure 14 shows the computed heat source intensity when the data has a 5% level of noise. In this case, the computed values are less stable but still relatively close to the true value. Also, as shown in Figure 15, the intensity of the inactive sources is correctly assigned, so the ability of the numerical method on finding the correct active source has not changed.

Finally, Figures 16 and 17 show the behavior of the proposed numerical method when the noise level of the temperature data is 10%. In this case, an optimal value of the Tikhonov parameter, $\lambda$, would yield more stable results; however, it is important to highlight how the numerical method is able to correctly differentiate between the active source and the inactive ones.

For the various cases, the elapsed time in the numerical solution of the inverse problem was about 20–40 s, proving the ability of the method to be applied in real-time applications. The numerical results are obtained with an implementation of the proposed method in Matlab [35] running in a ACER Aspire laptop, equipped with processor Intel Core i7-7500U 2.7 GHz, 12 GB of DDR4 RAM, and operative system Windows 10 (64 bit).

## 5 | Conclusions

This paper presents an inverse heat source problem arising from person localization in indoor spaces. The proposed method used to solve this problem is based on an integral representation for the temperature function. This representation is obtained from the knowledge of the Green function of the heat operator with

prescribed boundary conditions, and such Green's function is obtained through the use of the Laplace transform. Moreover, in this representation, the source function is approximated by a linear combination of the Gaussian functions, which allows an important simplification of the temperature function. The inverse heat source problem has been formulated as a system of integral equations, whose solution has been obtained by using the Tikhonov regularization procedure. The proposed method has been tested and validated with some numerical experiments, confirming its capability to accurately solve the inverse heat source problem. Indeed, the experiments show good agreement between the computed and actual source intensities, with relative errors kept at acceptable levels.

The promising results obtained in this paper encourage us to improve this method and to extend this study to slightly different domains or more complex heat source configurations. Finally, the method should be tested in real-world applications like the one in the living sector, where the proposed problem has been considered to localize persons within indoor spaces [20, 36]. To this aim, sensor noise, convective effects, and other uncertainties as windows, doors and room furniture should be evaluated and considered in the inversion procedure.

### Author Contributions

**Simonetta Boria:** writing – review and editing, project administration. **Nadaniela Egidi:** writing – review and editing, writing – original draft, validation, data curation. **Lorella Fatone:** writing – original draft, writing – review and editing, validation, data curation, visualization. **Josephin Giacomini:** writing – original draft, writing – review and editing, data curation, investigation. **Pierluigi Maponi:** conceptualization, investigation, methodology, writing – review and editing, writing – original draft, validation, data curation, supervision, formal analysis, funding acquisition. **Riccardo Piombin:** conceptualization, investigation, writing – original draft, writing – review and editing, visualization, validation, methodology, software, data curation, resources.

### Acknowledgments

Nadaniela Egidi, Lorella Fatone, Josephin Giacomini, and Pierluigi Maponi are members of the Gruppo Nazionale Calcolo Scientifico - Istituto Nazionale di Alta Matematica (GNCS - INdAM). Open access publishing facilitated by Universita degli Studi di Camerino, as part of the Wiley - CRUI-CARE agreement.

### Conflicts of Interest

The authors declare no conflicts of interest.

### References

1. Z. Qu, P. Jiang, and W. Zhang, "Development and Application of Infrared Thermography Non-Destructive Testing Techniques," *Sensors* 20 (2020): 38–51.

2. A. El Badia and T. Ha-Duong, "On an Inverse Source Problem for the Heat Equation. Application to a Pollution Detection Problem, II," *Journal of Inverse and Ill-Posed Problems* 10 (2002): 589–599.

3. H. Orlande, "Inverse Problems in Heat Transfer: New Trends on Solution Methodologies and Applications," in *International heat transfer conference* (2010), 379–398.

4. Y. Wang and P. Mendez, "Isotherm Penetration Depth Under a Moving Gaussian Surface Heat Source on a Thick Substrate," *International Journal of Thermal Sciences* 172 (2022): 107334.

5. Y. Xu, X. Zhang, J. Shen, and T. Shi, "Temperature Behavior of Metal Surface With Moving Annular Hollow Laser Heat Source," *Journal of Laser Applications* 32 (2020): 042014.

6. D. Zhong, S. Li, F. Weng, and M. Zhu, "Localization of Unsteady Heat Source in a Tube From Pressure Measurements With the Inverse Method," *Proceedings of the Combustion Institute* 36 (2017): 3733–3741.

7. S. Beddiaf, L. Autrique, L. Perez, and J. C. Jolly, "Heating Sources Localization Based on Inverse Heat Conduction Problem Resolution," *IFAC Proceedings Volumes* 45 (2012): 404–409.

8. M. B. Cherick, J. G. Bauzin, A. Hocine, Z. Peter, and N. Laraqi, "Detection of Surface Moving Heat Source Using Experimental Temperature Measurements on the Opposite Surface and Inverse Techniques," *International Journal of Heat and Mass Transfer* 219 (2024): 124840.

9. A. Prilepko and D. Tkachenko, "Well-Posedness of the Inverse Source Problem for Parabolic Systems," *Differential Equations* 40 (2004): 1540–1547.

10. A. Tikhonov and V. Arsenin, *Solutions of Ill-Posed Problems*, Winston. first ed. (Winston, 1977).

11. H. Engl, M. Hanken, and A. Neubauer, *Regularization of Inverse Problems*, first ed. (Springer, 2000).

12. P. Hansen, *Rank-Deficient and Discrete Ill-Posed Problems: Numerical Aspects of Linear Inversion*, first ed. (Society for Industrial and Applied Mathematics, 1998).

13. M. Ozisik and H. Orlande, *Inverse Heat Transfer: Fundamentals and Applications*, first ed. (Taylor and Francis, 2000).

14. C. Yang, "Solving the Two-Dimensional Inverse Heat Source Problem Through the Linear Least-Squares Method," *International Journal of Heat and Mass Transfer* 2 (1998): 393–398.

15. A. Shidfar, A. Zakeri, and A. Neisi, "A Two-Dimensional Inverse Heat Conduction Problem for Estimating Heat Source," *International Journal of Mathematics and Mathematical Sciences* 10 (2005): 1633–1641.

16. T. Min, S. Zang, and S. Chen, "Source Strength Identification Problem for the Three-Dimensional Inverse Heat Conduction Equations," *Inverse Problems in Science and Engineering* 28 (2020): 827–838.

17. Z. Masouri, E. Babolian, and S. Hatamzadeh-Varmazyar, "An Expansion-Iterative Method for Numerically Solving Volterra Integral Equation of the First Kind," *Computers and Mathematics with Applications* 59 (2010): 1491–1499.

18. P. Lamm and L. Elden, "Numerical Solution of First-Kind volterra Equations by Sequential Tikhonov Regularization," *SIAM Journal on Numerical Analysis* 34 (1997): 1432–1450.

19. P. Lamm, *A Survey of Regularization Methods for First-Kind Volterra Equations* (Springer Vienna, 2000).

20. S. Summa, S. Boria, N. Egidi, et al. "Indoor Spatial Tracking of Users Through a Grid of Thermocouples Installed on the Ceiling". submitted. 2024.

21. N. Egidi, J. Giacomini, and P. Maponi, "Inverse heat Conduction to Model and Optimise a Geothermal Field," *Journal of Computational and Applied Mathematics* 423 (2023): 114957.

22. V. Vladimirov, *Equations of Mathematical Physics* (Marcel Dekker, Inc., 1971).

23. K. Cole, A. Haji-Sheikh, J. Beck, and B. Litkouhi, *Heat Conduction Using Green's Functions*, second ed. (CRC Press, 2011).

24. M. Abramowitz and I. Stegun, *Handbook of Mathematical Functions*, ninth ed. (Dover Publications, 1972).

25. H. Carslaw and J. Jaeger, *Conduction of Heat in Solids*, second ed. (Clarendon Press, 1959).

26. K. Atkinson, *An Introduction to Numerical Analysis*, second ed. (John Wiley and Sons, 1989).

27. H. Wendland, *Scattered Data Approximation*, first ed. (Cambridge University Press, 2004).

28. T. Kik, "Heat Source Models in Numerical Simulations of Laser Welding," *Materials* 13 (2020): 2653.

29. J. Guo, P. Le Masson, E. Artioukhine, et al., "Estimation of a Source Term in a Two-Dimensional Heat Transfer Problem: Application to an Electron Beam Welding," *Inverse Problems in Science and Engineering* 14 (2006): 21–38.

30. C. Du, H. Yu, and L. Yu, "A Scale-Sensitive Heatmap Representation for Multi-Person Pose Estimation," *IET Image Processing* 16 (2022): 1194–1207.

31. R. Courant, K. Friedrichs, and H. Lewy, "On the Partial Difference Equations of Mathematical Physics," *IBM Journal of Research and Development* 11 (1967): 215–234.

32. T. Coleman and Y. Li, "A Reflective Newton Method for Minimizing a Quadratic Function Subject to Bounds on Some of the Variables," *SIAM Journal on Optimization* 6 (1996): 1040–1058.

33. Matlab, "Documentation of the lsqlin Method." (2024), accessed November 27, 2024. https://www.mathworks.com/help/optim/ug/lsqlin.html

34. V. Morozov, *Methods for Solving Incorrectly Posed Problems*, first ed. (New York Springer Verlag, 1984).

35. Matlab, "Matlab Documentation." (2024), accessed November 27, 2024. https://it.mathworks.com/help/matlab/index.html?lang=en

36. S. Boria, N. Egidi, L. Fatone, J. Giacomini, P. Maponi, and R. Piombin, "Improved Computational Techniques for Heat Sources Localization," *Mathematical Methods for Engineering Applications* 490 (2025): 157–169.